# Highly sensitive spectral interferometric four-wave mixing microscopy near the shot noise limit and its combination with two-photon excited fluorescence microscopy

**Keisuke Isobe, Yasuyuki Ozeki, Takehito Kawasumi, Shogo Kataoka, and Shin'ichiro Kajiyama**

*Department of Material and Life Science, Graduate School of Engineering, Osaka University, 2-1, Yamadaoka, Suita, Osaka 565-0871, Japan*
isobe@photonics.mls.eng.osaka-u.ac.jp

http://www-photonics.mls.eng.osaka-u.ac.jp

**Kiichi Fukui**

*Department of Biotechnology, Graduate School of Engineering, Osaka University, 2-1, Yamadaoka, Suita, Osaka 565-0871, Japan*

**Kazuyoshi Itoh**

*Department of Material and Life Science, Graduate School of Engineering, Osaka University, 2-1, Yamadaoka, Suita, Osaka 565-0871, Japan*

**Abstract:** We present spectral interferometric four-wave mixing (FWM) microscopy with a nearly shot-noise limited sensitivity and with the capability of separating FWM signals from fluorescence signals. We analyze the requirements for obtaining the shot-noise limited sensitivity and experimentally achieve the sensitivity that is only 4-dB lower than the shot-noise limit. Moreover, we show that only FWM signals can be extracted through the Fourier filtering even when the FWM spectrum is overlapped and overwhelmed by the fluorescence spectrum. We demonstrate simultaneous acquisition of FWM and two-photon excited fluorescence images of fluorescent monodispersed polystyrene microspheres.



**OCIS codes:** (180.6900) Three-dimensional microscopy; (300.6290) Spectroscopy, four-wave mixing; (190.4410) Nonlinear optics, parametric processes; (300.1030) Absorption; (320.7110) Ultrafast nonlinear optics.

## References and links

1. R. Hellwarth and P. Christensen, "Nonlinear optical microscopic examination of structure in polycrystalline ZnSe," Opt. Commun. **12**, 318-322 (1974).
2. J. N. Gannaway and C. J. R. Sheppard, "Second-harmonic imaging in the scanning optical microscope," Opt. and Quant. Elec. **10**, 435-439 (1978).
3. Y. Barad, H. Eisenberg, M. Horowitz, and Y. Silberberg, "Nonlinear scanning laser microscopy by third harmonic generation," Appl. Phys. Lett. **70**, 922-924 (1997).
4. M. Müller, J. Squier, K. R. Wilson, and G. J. Brankenhoff, "3D microscopy of transparent objects using third-harmonic generation," J. Microsc. **191**, 266-274 (1998).
5. M. D. Duncan, J. Reintjes, and T. J. Manuccia, "Scanning coherent anti-Stokes Raman microscope," Opt. Lett. **7**, 350-352 (1982).
6. A. Zumbusch, G. R. Holtom and X. S. Xie, "Three-dimensional vibrational imaging by coherent anti-Stokes Raman scattering," Phys. Rev. Lett. **82**, 4142-4145 (1999).

#75243 - $15.00 USD Received 19 September 2006; revised 22 October 2006; accepted 24 October 2006

7. K. Isobe, S. Kataoka, R. Murase, W. Watanabe, T. Higashi, S. Kawakami, S. Matsunaga, K. Fukui, and K. Itoh, "Stimulated parametric emission microscopy," Opt. Express **14**, 786-793 (2006).
8. L. Moreaux, O. Sandre, M. Blanchard-Desce, and J. Mertz, "Membrane imaging by simultaneous second-harmonic generation and two-photon microscopy," Opt. Lett. **25**, 320-322 (2000).
9. A. Zoumi, A. Yeh, and B. J. Tromberg, "Imaging cells and extracellular matrix in vivo by using second-harmonic generation and two-photon excited fluorescence," Proc. Natl. Acad. Sci. USA **99**, 11014-11019 (2002).
10. M. Kobayashi, K. Fujita, O. Nakamura, and S. Kawata, "Time-gated imaging for multifocus second-harmonic generation microscopy," Rev. Sci. Inst. **76**, 073704-1-073704-4 (2005).
11. R. K. Chang, J. Ducuing, and N. Bloembergen, "Relative phase measurement between fundamental and second-harmonic light," Phys. Rev. Lett. **15**, 6-9 (1965).
12. G. Marowsky, and G. Lüpke, "CARS-background suppression by phase-controlled nonlinear interferometry," Appl. Phys. B **51**, 49-51 (1990).
13. Y. Jiang, I. Tomov, Y. Wang, and Z. Chen, "Second-harmonic optical coherence tomography," Opt. Lett. **29**, 1090-1092 (2004).
14. C. Vinegoni, J. S. Bredfeldt, and D. L. Marks, "Nonlinear optical contrast enhancement for optical coherence tomography," Opt. Express **12**, 331-341 (2004).
15. K. Isobe, W. Watanabe, and K. Itoh, "Interferometric second-harmonic-generation microscopy," in Optics Japan 2002 Extended Abstracts (Optical Society of Japan (Japanese Society of Applied Physics), Tokyo, 2002), pp. 18-19.
16. S. Yazdanfar, L. H. Laiho, and P. T. C. So, "Interferometric second harmonic generation microscopy," Opt. Express **12**, 2739-2745 (2004).
17. E. O. Potma, C. L. Evans, and X. S. Xie, "Heterodyne coherent anti-Stokes Raman scattering (CARS) imging," Opt. Lett. **31**, 241-243 (2006).
18. C. L. Evans, E. O. Potma, and X. S. Xie, "Coherent anti-Stokes Raman scattering spectral interferometry: determination of the real and imaginary components of nonlinear susceptibility $\chi^{(3)}$ for vibrational microscopy," Opt. Lett. **29**, 2923-2925 (2004).
19. M. V. Sarunic, B. E. Applegate, and J. A. Izatt, "Spectral domain second-harmonic optical coherence tomography," Opt. Lett. **30**, 2391-2393 (2005).
20. G. W. H. Wurpel, J. M. Schins and M. Müller, "Direct measurement of chain order in single lipid mono- and bilayers with multiplex CARS," J. Phys. Chem. B **108**, 3400-3403 (2004).
21. J. F. de Boer, B. Cense, B. H. Park, M. C. Pierce, G. J. Tearney, and B. E. Bouma, "Improved signal-to-noise ratio in spectral-domain compared with time-domain optical coherence tomography," Opt. Lett. **28**, 2067-2069 (2003).
22. R. Leitgeb, C. K. Hitzenberger, and A. F. Ferchar, "Performance of Fourier domain vs. time domain optical coherence tomography," Opt. Express **11**, 889-894 (2003).
23. R. Adair, L. L. Chase, and S. A. Payne, "Nonlinear refractive index of optical crystal," Phys. Rev. B **39**, 3337-3350 (1989).
24. P. T. So, C. Y. Dong, B. R. Masters and K. M. Berland, "Two-photon excitation fluorescence microscopy," Annu. Rev. Biomed. Eng. **2**, 399-429 (2000).

## 1. Introduction

In the recent biological research field, there is a growing demand for the development of high-resolution, three-dimensional imaging tools for exploring the underlying biological functions. For this purpose, a variety of coherent nonlinear-optical microscopies have been proposed and demonstrated [1-7]. They are based on various nonlinear phenomena such as second-harmonic generation (SHG) [1, 2], third-harmonic generation (THG) [3, 4], and four-wave mixing (FWM) including coherent anti-Stokes Raman scattering (CARS) [5, 6] and stimulated parametric emission (SPE) [7]. A common advantage of these techniques is the capability of three-dimensional sectioning of samples without staining. It is also reported that the combination of coherent nonlinear microscopy and fluorescence microscopy is a powerful tool for obtaining informative images of biomedical samples [8, 9].

One of important issues in nonlinear optical microscopy is that the sensitivity is severely limited because the optical signal is generated through a nonlinear process, which is typically weak and occurs in a limited volume. It is true that one can enhance the signal power to some extent by increasing the optical power incident on a sample. However, the effect of such an intense, focused optical pulse on the viability of living samples seems to be still an open question. Another possible way to improve the sensitivity is to utilize an optical detector with

#75243 - $15.00 USD Received 19 September 2006; revised 22 October 2006; accepted 24 October 2006

high sensitivity. In particular, considering that signal-to-noise ratio (SNR) of a weak optical signal is typically limited by shot noise, it would be advantageous if we could achieve shot-noise limited detection. When the detection is shot-noise limited, the number of signal photons, which is required for achieving a desired SNR, is the smallest. As a result, one can reduce the integration time or the optical power incident on the sample.

In previous experiments of nonlinear microscopy, photomultipliers, avalanche photodiodes and cooled/intensified charge-coupled devices (CCDs) have been used to realize sensitive photo-detection, while special attentions have to be paid therein to reduce dark current and stray light. As a result, it is quite difficult to achieve nearly shot-noise limited sensitivity with these detectors. Moreover, these detectors are also sensitive to fluorescence signals, which sometimes overwhelm the nonlinear signals and prohibit the above-mentioned combination of nonlinear- and fluorescence-microscopy. Although this problem could be solved by introducing a time-gating circuit [10], it may result in an increased complexity of the electronic circuits and/or a degraded SNR due to the loss of a part of the nonlinear signal.

Another interesting technique is an interferometric detection, where a weak signal electric field is mixed with an intense local oscillator (LO) field and their interference signal is detected with an optical detector with a moderate sensitivity. It is theoretically known that the shot-noise limited detection would be possible with this technique. Furthermore, fluorescence signals may be almost completely removed because the fluorescence signals are incoherent and do not interfere coherently with the LO signal. Historically, the nonlinear interferometric technique in time domain was first proposed by Chang *et al*. in as early as 1965 [11], where SHG signals were detected for measuring the complex second-order susceptibility of various semiconductor materials. Similar techniques were used for separating resonant CARS signals from nonresonant CARS signals [12] and applied to imaging systems [13-17]. Another version of interferometric detection technique is spectral interferometry, where two signals are mixed with different temporal delays and the resultant spectral fringe pattern is detected with a spectrometer. This technique was introduced for the determination of the real and imaginary parts of nonlinear susceptibility [18] and applied to spectral domain SHG-optical coherence tomography (OCT) [19]. In spite of these numerous reports on the interferometric detection of nonlinear signals, there has been almost no report which fully exploits the above-mentioned advantages (i.e. shot-noise limited detection and fluorescence removal). A possible reason is that it is difficult to generate a sufficiently intense LO signal, which has to be generated through the weak nonlinear process similarly to the sample signal. We note that the shot-noise limited detection itself has already been achieved in CARS microscopy by using signal enhancement through the interference between CARS signal and background LO signal, both of which are generated in a same focal volume [20]. However, a highly sensitive CCD has to be employed therein due to the weak intensity of the LO signal. Moreover, the fluorescence signal cannot be separated in this scheme.

In this paper, we experimentally demonstrate spectral interferometric four-wave mixing (SI-FWM) microscopy with a nearly shot-noise limited sensitivity and the capability of fluorescence removal. We show analytically that proper setting of the integration time of the optical detector is crucial for realizing the shot-noise limited detection, especially when one uses a CCD with a moderate sensitivity. In the experiment, we show that the sensitivity of our microscope is only 4-dB lower than the shot-noise limit, proving the high sensitivity of this technique. Moreover, we experimentally confirm that the heterodyne detection enables us to separate the FWM signals from the fluorescence signals. We finally demonstrate simultaneous acquisition of the FWM and two-photon excited fluorescence (TPEF) signals for obtaining images of fluorescence beads. The structure of this paper is as follows. We start in Section 2 with a discussion of the SNR in the shot-noise limit. In Section 3, we report on the experiments of spectral interferometric FWM microscopy. In Section 4, we discuss the way to further improve our system. In Section 5, we summarize this paper.

#75243 - $15.00 USD Received 19 September 2006; revised 22 October 2006; accepted 24 October 2006

## 2. Theory of spectral interferometric FWM microscopy

We first summarize the principle of SI-FWM microscopy and then discuss the SNR in the shot-noise limit. Although the discussion is similar to that reported in Ref. 21, the theory presented here is derived in the unit of number of photo-carriers generated in a CCD, which is used in a spectrometer. Since the characteristics of commercially available CCD are often provided in this unit, our discussion is quite useful for the design of practical systems.

A schematic diagram of a SI-FWM microscope is shown in Fig. 1. Pump and probe pulses from a pulsed laser are lead to a first beam splitter (BS1), which splits the beam into two arms. One beam is lead to a FWM microscope, where pulses are focused into a sample under test. As a result of 3rd-order nonlinear optical effect in a sample, a FWM signal is generated. The other beam is lead to a local oscillator, where pulses are focused into a reference sample. A FWM signal from the reference sample is used as a LO signal. The two FWM signals are combined by a second beam splitter (BS2) with a delay difference of $\tau$. The spectral interference between the FWM signals is measured with a spectrometer, where the input signal is spectrally dispersed and each spectral component is converted to photo-carriers by a CCD. Here, the number of the photo-carriers per optical angular frequency is given by

$$K(\omega) = \frac{\eta\rho\Delta t}{2h\nu}\left[\left|E_S(\omega)\right|^2 + \left|E_{LO}(\omega)\right|^2 + 2\left|E_S(\omega)\right|\left|E_{LO}(\omega)\right|\cos\left(\omega\tau + \phi_S - \phi_{LO} + \phi_0\right)\right], \quad (1)$$

where $E_S(\omega)$ and $E_{LO}(\omega)$ are the Fourier-transformed electric fields of the sample FWM signal and the LO FWM signal, respectively, $\eta$ is quantum efficiency of the detector, $\rho$ is excess optical loss due to optical components such as lenses and diffraction grating, $\Delta t$ is integration time of the CCD, $h\nu$ is photon energy, $\phi_S$ and $\phi_{LO}$ are the phases of the sample FWM signal and the LO signal, respectively, and $\phi_0$ is phase offset due to the optical components. The factor 1/2 accounts for the intrinsic 3-dB optical loss of BS2. For simplicity, in this discussion we do not assume that the FWM processes have steep resonance. Consequently, we assume that $E_S(\omega)$ and $E_{LO}(\omega)$ are similar to each other and that $\phi_S - \phi_{LO}$ is constant over any $\omega$. Nevertheless, our discussion can be easily extended to include a resonant case.

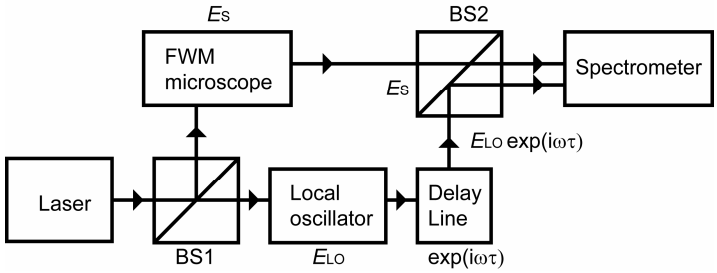


Fig. 1. Schematic diagram of a SI-FWM microscope.

Once $K(\omega)$ is measured with the spectrometer, the interference signal is obtained through the following procedure. First, we calculate the inverse Fourier transform (IFT) of $K(\omega)$, which is given by $\tilde{K}(t) = (2\pi)^{-1}\int K(\omega)e^{-i\omega t}d\omega$. Then we numerically extract the fringe component at $t = \tau$ and calculate its Fourier transform (FT) to obtain $S(\omega) = \int_{\tau-\Delta\tau/2}^{\tau+\Delta\tau/2}\tilde{K}(t)e^{i\omega(t-\tau)}dt$. Here, $\Delta t$ has to satisfy $\tau_{coh} << \Delta\tau << \tau$ where $\tau_{coh}$ is the coherence time of the FWM signals. Finally, the signal amplitude $S$ is given by

$$S \equiv \left|\int S(\omega)d\omega\right| = \frac{\eta\rho\Delta t}{2h\nu}\sqrt{P_S P_{LO}}, \quad (2)$$

where $P_S$ and $P_{LO}$ are optical powers of the sample FWM signal and the LO FWM signal, respectively.

#75243 - $15.00 USD Received 19 September 2006; revised 22 October 2006; accepted 24 October 2006

Next, we consider the shot noise of the interference signal. Assuming that the LO FWM signal is much stronger than the sample FWM signal, i.e., $|E_S(\omega)| << |E_{LO}(\omega)|$, the square average of the shot noise $K_{shot}(\omega)$ in the unit of number of photo-carriers per optical frequency is expressed as

$$\left\langle K_{shot}^2(\omega)\right\rangle = K(\omega) \sim \frac{\eta\rho\Delta t}{2h\nu}\left|E_{LO}(\omega)\right|^2, \tag{3}$$

where the bracket denotes the ensemble average. Then the square average of the shot-noise contribution can be derived as

$$\begin{aligned}\left\langle |N|^2\right\rangle &\equiv \left\langle \left|\int N(\omega)d\omega\right|^2\right\rangle = \left\langle \left|2\pi\tilde{K}_{shot}(\tau)\right|^2\right\rangle = \left\langle \left|\int K_{shot}(\omega)e^{-i\omega\tau}d\omega\right|^2\right\rangle \\ &= \left\langle \int K_{shot}^2(\omega)d\omega\right\rangle = \int\left\langle K_{shot}^2(\omega)\right\rangle d\omega = \frac{\eta\rho\Delta t}{2h\nu}P_{LO},\end{aligned} \tag{4}$$

where $N(\omega)$ is noise spectral density due to the shot noise and $\tilde{K}_{shot}(t) = (2\pi)^{-1}\int N(\omega)e^{-i\omega(t-\tau)}d\omega$ is the IFT of $K_{shot}(\omega)$. Since $N$ includes the same amount of amplitude noise $N_A$ and phase noise $N_P$, we obtain

$$\left\langle N_A{}^2\right\rangle = \frac{\eta\rho\Delta t}{4h\nu}P_{LO}. \tag{5}$$

From Eq. (2) and (5), the SNR in the shot-noise limit can be derived as

$$\mathrm{SNR}_{shot} = |S|^2 / \left\langle N_A{}^2\right\rangle = \frac{\eta\rho\Delta t P_S}{h\nu}. \tag{6}$$

This result is consistent with that derived for Fourier-domain OCT [21, 22]. In the shot-noise limited detection, the SNR is uniquely determined by the number of signal photons.

Here, we discuss the requirement for achieving the shot-noise limited sensitivity. This requirement is satisfied when the shot noise of each pixel dominates over other noise sources, such as Johnson noise $C_{thermal}$, readout noise $C_{read}$ and dark photo-carrier $C_{dark}$, all of which are expressed in the unit of number of photo-carriers. By defining $\Delta\omega$ as a spectral width corresponding to each pixel of the CCD, the shot noise of each detector is expressed as

$$\left\langle K_{shot}^2(\omega)\right\rangle\Delta\omega = K(\omega)\Delta\omega \sim \frac{\eta\rho\Delta t}{2h\nu}\left|E_{LO}(\omega)\right|^2\Delta\omega. \tag{7}$$

Since this value should be much larger than $C_{thermal}{}^2 + C_{read}{}^2$, we obtain the requirement given by

$$\Delta t >> \frac{2h\nu\left(C_{thermal}^2 + C_{read}^2\right)}{\eta\rho\left|E_{LO}(\omega)\right|^2\Delta\omega}. \tag{8}$$

which sets the lower limit of the integration time. Furthermore, in order to neglect the effect of dark current, $K(\omega)\Delta\omega >> C_{dark}$ should be satisfied. Consequently, we obtain

$$\frac{\eta\rho\left|E_{LO}(\omega)\right|^2\Delta\omega}{2h\nu} >> \frac{i_{dark}}{q}, \tag{9}$$

where $i_{dark}$ is dark current and $q$ is electron charge. Another obstacle for achieving the shot-noise limited sensitivity is the saturation of photo-carrier in the detector. To avoid this, $K(\omega)\Delta\omega < C_{max}$ should be satisfied, where $C_{max}$ denotes the maximum number of photo-carriers. As a result, we obtain

$$\Delta t < \frac{2h\nu C_{max}}{\eta\rho\left|E_{LO}(\omega)\right|^2\Delta\omega}. \tag{10}$$

#75243 - $15.00 USD Received 19 September 2006; revised 22 October 2006; accepted 24 October 2006

Based on the above discussion, we summarize the requirements for obtaining the shot-noise limited sensitivity in SI-FWM microscopy as follows. First, the integration time should be properly set so that Eqs. (8) and (10) are satisfied. Especially, Eq. (8) is quite important in SI-FWM microscopy where the available optical power of the LO signal is limited because the LO signal is generated through the weak nonlinear FWM process. This is compared to other linear interferometry techniques, where the LO signal with a sufficient optical power is directly obtained from the laser source. Second, the LO signal power has to be large enough to satisfy Eq. (9). Third, the resolution of spectrometer has to be sufficiently low (i.e. $\Delta\omega$ should be high) to relax the above two constraints. This is important typically for the imaging application, where small $\Delta t$ is preferred to shorten the acquisition time.

## 3. Experiment

We conducted experiments to demonstrate highly sensitive SI-FWM microscopy. A schematic of the experimental setup is shown in Fig. 2(a). As an excitation light source, we used a broadband mode-locked Ti:sapphire laser (Nanolayers, Venteon). The temporal duration and the repetition rate of the output pulses were $\leq 8$ fs and 200 MHz, respectively. The spectrum of the laser pulse ranged from 650 to 950 nm as shown in Fig. 2(b). Taking advantage of such a broadband spectrum, we utilized the intra-pulse FWM effect, where three frequency components ($\omega_1$, $\omega_2$, $\omega_3$) in a single pulse, which acted as two pump pulses and a probe pulse, were mixed through the 3rd-order nonlinearity to generate a FWM field at $\omega_4 = \omega_1 + \omega_2 - \omega_3$. In this particular experiment, $\omega_4$ was measured to be approximately $2\pi \times 501$ Trad/s (598 nm). We estimate that the pump ($\omega_1$ and $\omega_2$) and probe ($\omega_3$) wavelengths were approximately 690 nm and 816 nm, respectively. This estimation is based on the fact that the pulse at the focal spot was highly distorted by 3rd- and higher order dispersions of optical components and that we could obtain a 374-nm pulse through sum-frequency generation of pump and probe components of the focused pulse. It is also noted that the origin of FWM signal in this experiment was mainly electronic 3rd-order nonlinearity. We did not observe steep resonance due to CARS.

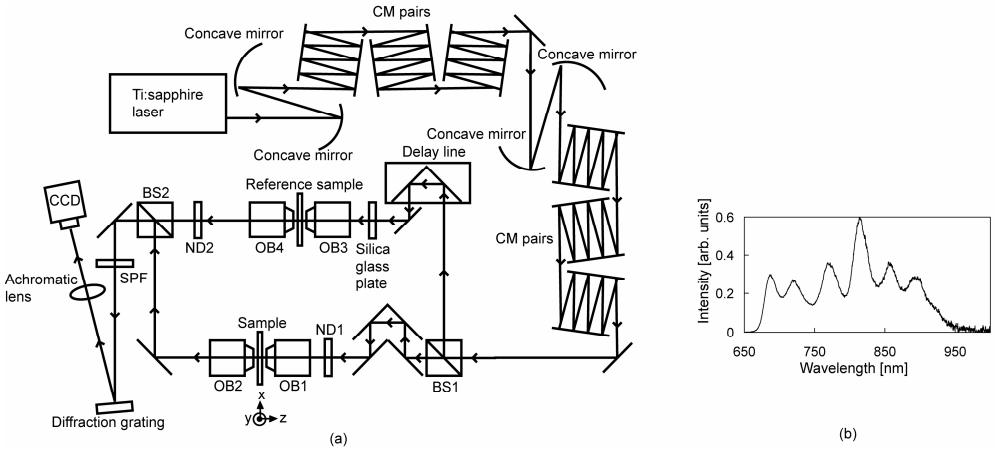


Fig. 2. Experimental setup of SI-FWM microscopy. CM: chirp mirror, BS: beam splitter, OB: objective lens, SPF: short-pass filter, CCD: charge coupled device.

In order to pre-compensate for the second-order dispersion of the optical components, the laser pulses passed through chirp mirror pairs. Then the pulses were lead to an interferometer which is similar to that shown in Fig. 1. In the sample arm, the beam was focused into a sample by an objective lens (OB1). The FWM field generated in the sample was collimated by OB2. The sample was moved with respect to the focal spot by a three-axis piezoelectric transducer (PZT) stage. In the reference arm, the laser beam was focused by OB3 into a slide

#75243 - $15.00 USD Received 19 September 2006; revised 22 October 2006; accepted 24 October 2006

glass to generate a LO-FWM field, which was collimated by OB4. The numerical aperture of all objective lenses was 0.6. In order to introduce a temporal delay between the FWM fields from the sample and the reference sample, we inserted an optical delay line. To compensate for the difference of the second-order dispersions between the two arms, a silica-glass plate was inserted before OB3. A variable neutral density filter (ND1) was placed before OB1 for controlling the power incident to the sample. Another one (ND2) was placed after OB4 for adjusting the LO power. The two FWM fields were overlapped in space on a second beam splitter (BS2) with a delay difference of 130 fs. In order to reject residual pump and probe beams and to extract the FWM fields, we inserted short-pass filters (SPFs). Then the FWM fields were spectrally dispersed by a diffraction grating (600 line/mm) and focused by an achromatic lens onto a line CCD (Hamamatsu Photonics, C9047-01), on which the two FWM fields interfered and yielded the interference signal. To obtain the shot-noise limited sensitivity, we determined the integration time of the CCD as follows. According to the data sheet and catalog specifications of the CCD, the root-mean-square value of Johnson and readout noises $\sqrt{C_{\text{thermal}}^2 + C_{\text{read}}^2}$ was $3.2 \times 10^2$, $i_{\text{dark}}/q$ was $4.0 \times 10^3$ $\text{s}^{-1}$, $C_{\max}$ was $6.0 \times 10^5$ and $\eta$ was 0.92. As for the experimental parameters, the resolution of the spectrometer $\Delta\omega$ was 2.7 Trad/s, $\rho$ was 0.38 and $h\nu$ was $3.3 \times 10^{-19}$ J and the maximum power spectral density of the LO was $5.1 \times 10^{-23}$ W/rad. By substituting these values in Eqs. (8)-(10), we obtained 1.4 ms $<< \Delta t <$ 8.2 ms, while Eq. (9) was fully satisfied. Therefore, integration time was set to 2-8 ms.

We first measured the emission spectrum from each arm. The spectrum was obtained by blocking the other arm. The sample under test was a dye (Coumarin 120, 6 mM) dissolved in ethanol. The integration time was set to 8 ms. The incident pulse energy was set to $2.0 \times 10^2$ pJ which corresponds to an average power of 40 mW. The emission spectra of the dye solution and the slide glass are shown in Figs. 3(a) and (b), respectively. In both figures, spectral peaks at 598 nm due to the FWM signals were present. On the other hand, a broad peak ranging from 390 to 570 nm appeared only in Fig. 3(a). This is TPEF signal, as will be confirmed later. Figure 3(c) shows a spectral interferogram obtained by mixing the signals from the dye solution and the slide glass. It is clearly seen that the fringe pattern was not present in the spectral region of the TPEF signal and but was present only in the spectral region of the FWM signal. In this way, the selective detection of the FWM signal was achieved.

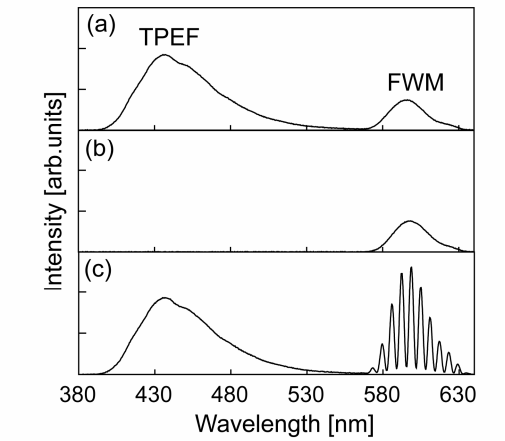


Fig. 3. Emission spectra and spectral interferogram. (a) Emission spectrum from a dye (Coumarin 120, 6 mM) dissolved in ethanol. (b) Emission spectrum obtained from a slide glass. (c) Spectral interferogram of (a) and (b).

Next, we investigated the dependences of the FWM and TPEF signal intensities on the incident intensity. The intensities of the FWM and TPEF signals were calculated by

#75243 - $15.00 USD Received 19 September 2006; revised 22 October 2006; accepted 24 October 2006

integrating the spectra in the range from 582 to 634 nm and in that from 393 to 561 nm, respectively. The result is shown in Fig. 4. The slopes were found to be 3.00 and 1.98 for the FWM (triangle) and TPEF (square) signal intensities, respectively. In this way, we confirmed that the FWM and TPEF signals were generated by three and two photons, respectively.

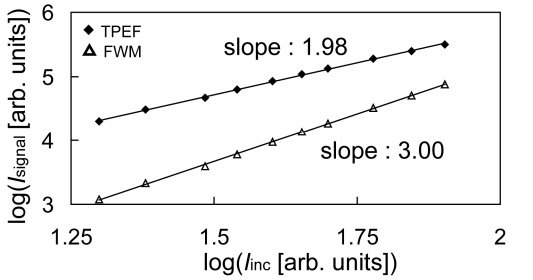


Fig. 4. Dependences of FWM (triangle) and TPEF (square) signal intensities $I_{signal}$ on incident intensity $I_{inc}$.

In order to confirm the signal amplification through the heterodyne mixing, we measured the interferometric signal as a function of the LO power. The incident pulse energy was set to 24 pJ which corresponds to an average power of 4.8 mW. The result is shown in Fig. 5(a) in a log-log scale. The slope was found to be 0.50, which agreed well with Eq. (2).

We next measured the SNR of the interferometric signal according to the following procedure. The spectral interferograms were recorded 500 times by fixing the sample position. Then the square average and the variance of the interferometric signals were calculated to obtain the SNR. We used a part of spectrum ranging from 570 to 635 nm. The integration time was set to 8 ms in such a way that the Johnson and readout noises were neglected as mentioned above. The incident pulse energies were set to (i) 23 pJ and (ii) 17 pJ which correspond to average powers of (i) 4.6 mW and (ii) 3.4 mW, respectively. The powers $P_S$ of the FWM field from the dye solution were estimated through the direct detection of FWM signals with the CCD and found to be (i) 782 fW and (ii) 314 fW, respectively, considering the quantum efficiency and optical loss. The SNR in the direct detection were as small as (i) 5.86 and (ii) 5.20 dB, respectively. The theoretical limits of the SNR were calculated to be (i) 38.2 dB and (ii) 34.3 dB, respectively. As shown in Fig. 5(b), the SNR was improved as the LO power was increased. At last, the SNR converged on constant values, which were only 4-dB lower than the shot-noise limited SNR. This is the *direct indication* that near-shot-noise-limited sensitivity has been successfully achieved.

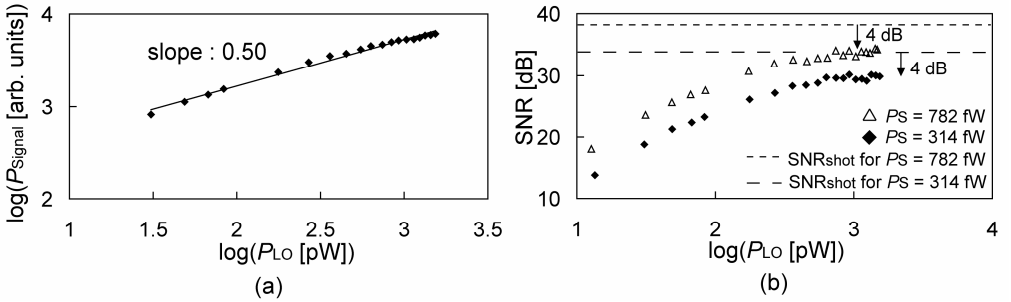


Fig. 5. Dependences of interferometric signal $P_{signal}$ (a) and SNR (b) on the LO power $P_{LO}$.

To compare the heterodyne spectral interferometric detection with the direct detection of the FWM signal, we observed a one-dimensional (1D) distribution of the FWM signal near the interface between a slide glass and air. The slide glass was scanned with a step size of 50 nm in the depth (i.e. *z*) direction (see Fig. 2(a)). The incident pulse energy and average power

#75243 - $15.00 USD Received 19 September 2006; revised 22 October 2006; accepted 24 October 2006

were 8.0 pJ and 1.6 mW, respectively. As shown in Figs. 6(a) and (b), the effect of the signal amplification is dramatic. The interface between the slide glass and air can be found in Fig. 6(a) but not in Fig. 6(b). The SNR in the heterodyne detection was 21.5 dB, while that in the direct detection was less than 0 dB and the signals were completely buried in noises. This result shows that the heterodyne spectral interferometric detection improved the SNR without increasing the integration time as compared with the direct detection of the FWM signal.

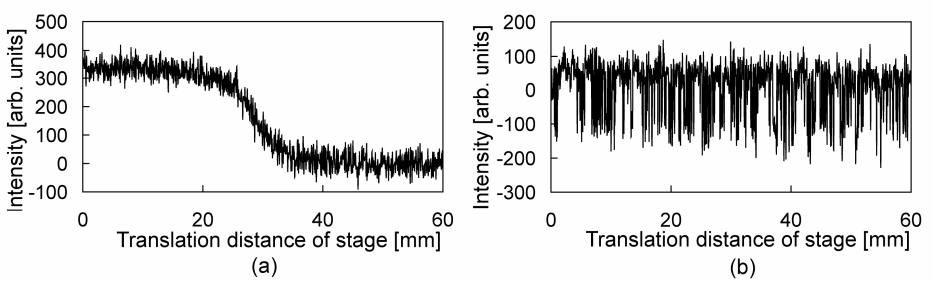


Fig. 6. One-dimensional distribution of FWM signal near the interface between the slide glass and air. The traces were measured with (a) heterodyne spectral interferometric detection and (b) direct detection.

Next, we demonstrate the separation of FWM signals from fluorescent signals. Figure 7(a) shows the emission spectrum from mixed dye solution (Coumarin 120 and Coumarin 153). It was found that the FWM spectrum (from 570 to 640 nm) was overlapped and almost overwhelmed by the TPEF spectrum (from 480 to 640 nm) from the Coumarin 153. Nevertheless, as shown in Fig. 7(b), a fringe pattern was found in the spectral region of the FWM signal. Then the FWM spectrum was extracted through the Fourier filtering as shown in Fig. 7(c). In this way, the heterodyne detection enables us to remove the fluorescence signals without losing the FWM signals.

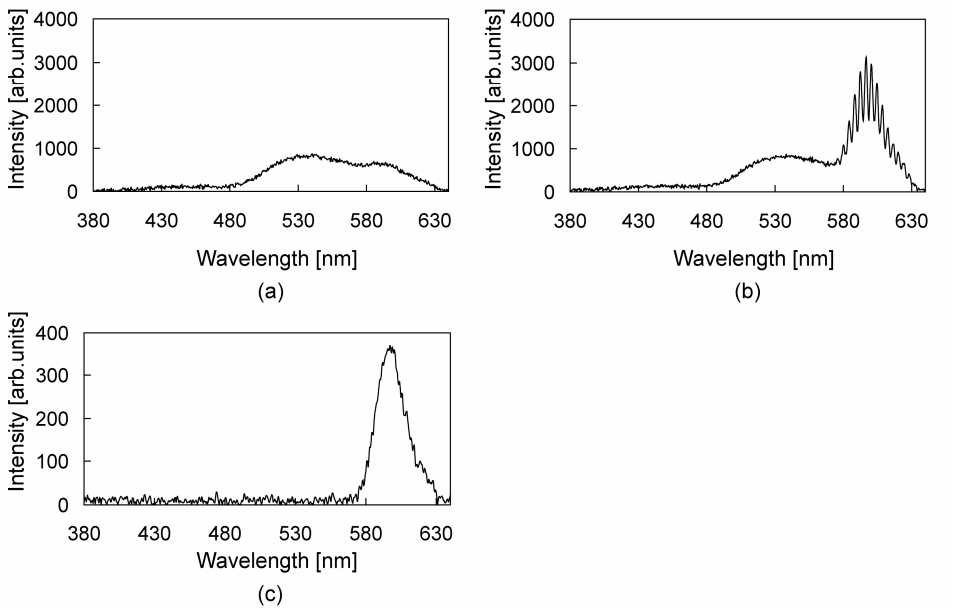


Fig. 7. Emission spectra from the mixed dye solution (Coumarin 120 and Coumarin 153). (a) Emission spectrum in the direct detection. (b) Spectral interferogram. (c) Reconstructed FWM spectrum.

#75243 - $15.00 USD Received 19 September 2006; revised 22 October 2006; accepted 24 October 2006

Finally, in order to investigate the practical applicability of spectral interferometric FWM microscopy, we demonstrated simultaneous acquisition of FWM and TPEF images. The sample was fluorescent monodispersed polystyrene microsphere (Polysciences, Inc, fluoresbrite carboxy BB microspheres). The excitation peak wavelength was 360 nm, the emission peak wavelength was 407 nm, and the diameter was 6 μm. The sample was scanned with a step size of 0.4 μm in the *xy* plane (see Fig. 2(a)). The image size was 65 × 65 pixels. The incident pulse energy and average power were 14 pJ and 2.8 mW, respectively. The integration time for each pixel was reduced to 2 ms. As a result, the sensitivity may have been slightly lower than the shot-noise limit but still higher than the direct detection. Figs. 8(a) and (b) show the cross-sectional images obtained with (a) the interferometric FWM signal and (b) the TPEF signal. In this way, we successfully obtained both images, which would be useful for application to biomedical imaging. However, a slight amount of dithering was observed due to the relatively long acquisition time (~33 s). To cope with this problem, we are currently trying to further decrease $\Delta t$. In the next section, we discuss possible ways to decrease $\Delta t$.

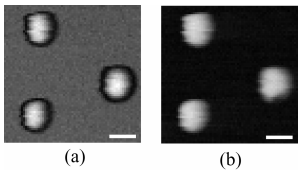


Fig. 8. Simultaneously obtained Images of fluorescent microbeads. (a) Interferometric FWM image. (b) TPEF image. Scale bar indicates 5 μm.

## 4. Discussion

As shown in the above experiment, our SI-FWM microscopy has nearly shot-noise limited sensitivity. However, the integration time has to be as long as several milliseconds to compensate for the insufficiency of the LO power. This leads to relatively long image acquisition time (~33 s for 65 × 65 pixels). To cope with this problem and realize real-time visualization, we consider the following two methods. The first one is to reduce the spectral resolution of the spectrometer. We are aware of the fact that the resolution of the spectrometer is much higher than that is required for resolving the spectral fringe and there is a room to reduce the resolution by approximately 10 times. This would allow us to shorten the integration time by the same factor. The other one is to increase the LO power by employing a reference sample with a high 3$^{rd}$-order susceptibility. If a semiconductor material such as cadmium sulfide (CdS) could be used as a reference sample, the LO power could be increased by approximately $3 \times 10^5$ times since the 3$^{rd}$-order susceptibility of CdS is approximately 600 times larger than that of the fused silica [23]. Such a high LO power would be sufficient for shortening the integration time and realizing real-time imaging.

On the other hand, it should be noted that the SNR is also proportional to the integration time when the sensitivity is shot-noise-limited. This would also limit the image acquisition rate. To cope with this, we are currently working to improve the FWM efficiency by compensating for 3$^{rd}$- and higher order dispersions of optical pulses. The result will be presented elsewhere.

## 5. Conclusion

In conclusion, we have demonstrated SI-FWM microscopy with a nearly shot-noise limited sensitivity. We discussed the requirements for obtaining shot-noise limited sensitivity and showed that the integration time has to be long enough to neglect Johnson and readout noises. This is quite important in SI-FWM microscopy where LO signal is weak. Considering these requirements, we experimentally achieved the sensitivity that was only 4-dB lower than the shot-noise limit. Moreover, we demonstrated that the heterodyne detection allows us to separate the FWM signals from the fluorescence signals, and the FWM and TPEF signals can be simultaneously used to image the sample. Thus, SI-FWM microscopy was shown to be a

#75243 - $15.00 USD Received 19 September 2006; revised 22 October 2006; accepted 24 October 2006

quite effective tool because of its enhanced sensitivity and its capability of combining FWM microscopy and fluorescence microscopy. In addition, this sensitivity enhancement is quite attractive for extending the penetration depth in scattering media, where the nonlinear optical imaging is typically limited to a few hundred micrometers from the surface [24]. It is also noted that our discussion can be directly applied to other nonlinear coherent microscopes with spectral interferometry.

**Acknowledgments**

This work was partly supported by a grant from the Cooperative Link of Unique Science and Technology for Economy Revitalization promoted by the Ministry of Education, Culture, Sports, Science and Technology, Japan. This work was also supported in part by SENTAN, JST (Japan Science and Technology Agency).

#75243 - $15.00 USD Received 19 September 2006; revised 22 October 2006; accepted 24 October 2006